Title

Self-assembly of precisely defined DNA nanotube superstructures using DNA origami seeds

Journal

Nanoscale, 9(2)

ISSN

2040-3364

Authors

Mohammed, AM
Velazquez, L
Chisenhall, A
et al.

Publication Date

2017-01-05

DOI

10.1039/c6nr06983e

Nanoscale

COMMUNICATION

View Article Online
View Journal | View Issue

Cite this: *Nanoscale*, 2017, **9**, 522

Received 2nd September 2016,
Accepted 5th December 2016

DOI: 10.1039/c6nr06983e

www.rsc.org/nanoscale

Self-assembly of precisely defined DNA nanotube superstructures using DNA origami seeds†

A. M. Mohammed,[a] L. Velazquez,[b] A. Chisenhall,[a] D. Schiffels,‡[b] D. K. Fygenson[b,c] and R. Schulman*[a,d]

We demonstrate a versatile process for assembling micron-scale filament architectures by controlling where DNA tile nanotubes nucleate on DNA origami assemblies. "Nunchucks," potential mechanical magnifiers of nanoscale dynamics consisting of two nanotubes connected by a dsDNA linker, form at yields sufficient for application and consistent with models.

A major goal of bottom-up synthesis is the self-assembly of integrated nanoscale devices.[1,2] One-dimensional structures are important primitives for such structures. For example, self-assembly of nanowires or carbon nanotubes into specific geometries could form electrical circuits.[3,4] Nanoscale tubular filaments could likewise assemble into machines and sensors, as demonstrated by the *in vivo* assembly of cytoskeletal structures such as the cilium[5] and the mitotic spindle.[6,7]

While the self-assembly of DNA,[8–12] peptides,[13,14] and other[15] types of filaments has been well-explored, relatively little is known about how to organize these filaments into architectures featuring precise numbers of components.[16] The ability to synthesize designed filament architectures could make it possible to construct molecular machines with new functions that can operate outside cells under a variety of physical and chemical conditions. In this paper we explore the assembly of DNA tile nanotubes into an elemental multi-filament architecture.

In vivo, cytoskeletal filaments are often arranged by controlling their nucleation using protein complexes such as Arp2/3[17,18] or the centriole[19] that template actin or microtubule growth. Analogously, formin[20] and the γ-tubulin small complex[21] can promote filament nucleation in specific regions of a cell to direct the formation of filament networks or bundles.

We have previously developed structures that nucleate DNA DAE-E tile nanotubes, termed nanotube seeds.[22] Here we use these structures to develop a biomimetic strategy for the creation of nanotube architectures, in which these seeds organize DNA tile nanotubes as they assemble. We demonstrate this strategy by self-assembling "DNA nanotube nunchucks" that consist of two nanotubes joined at their ends by a stretch of double-stranded DNA (dsDNA) of arbitrary length and sequence.

We assess the assembly of both *homogeneous* nunchucks, consisting of two connected nanotubes of identical tile types, and *heterogeneous* nunchucks, in which two nanotubes of distinct tile types are connected.

Our assembly strategy consists of linking DNA origami seeds end-wise with a synthetic stretch of dsDNA and then growing nanotubes from the opposite ends of the seeds. Previous attempts to form nunchucks by directly linking preformed DNA nanotubes endwise resulted in very low yields (<1%, data not shown).[23] The seed-based assembly strategy developed here produces these structures with dramatically higher yields (>40%).

DAE-E tile nanotubes typically self-assemble over the course of a thermal anneal in two stages (Fig. 1a). First, DAE-E tiles assemble from five component strands at a relatively high temperature (~45–65 °C).[8] Then, tile sticky ends hybridize to form nanotubes at a distinctly lower temperature (~40–30 °C), which depends on tile concentration. A nanotube seed is a DNA origami structure with 12 helices arranged into a hollow cylinder. Adapter strands on one end of the seed present sticky ends positioned so as to resemble a nanotube. Near the sticky-end melting temperature, nanotubes grow from seeds more rapidly than they nucleate spontaneously.[22] For our seeded assembly strategy, the thermal anneal involves a long incubation near the sticky-end melting temperature, such that most nanotubes grow from seeds.

Because seeds are DNA origami structures, it is possible to exercise exquisite control over how they attach to one another

[a]*Chemical and Biomolecular Engineering, Johns Hopkins University, USA. E-mail: rschulm3@jhu.edu*
[b]*Department of Physics, University of California Santa Barbara, USA*
[c]*Biomolecular Science and Engineering, University of California Santa Barbara, USA*
[d]*Computer Science, Johns Hopkins University, USA*

†Electronic supplementary information (ESI) available: DNA strand sequences, additional experimental methods and microscopy images. See DOI: 10.1039/c6nr06983e

‡Current address: Nanofabrication Research Group, Gaithersburg.

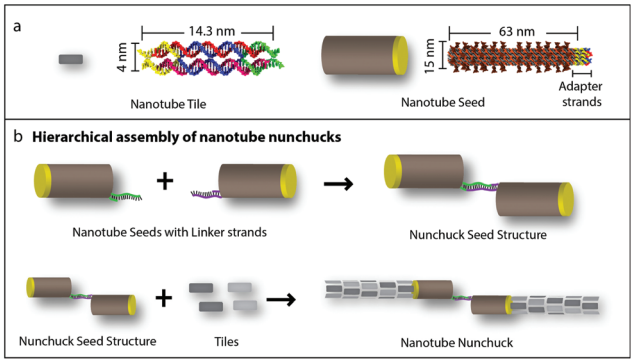

Fig. 1 Nanotube nunchuck design and assembly. (a) A DAE-E DNA nanotube tile consists of five DNA strands. Each strand is shown in a different color. Single-stranded sticky ends on four tile edges can hybridize to complementary sticky ends on other tiles to form nanotubes. A DNA origami nanotube seed consists of a long scaffold strand (M13mp18) that is assembled into a cylindrical shape by 72 staple strands. Hairpins on the outside of the seed ensure the structure curls in the correct direction during folding. Nanotubes grow from tile adapter strands on one side of the seed (yellow). (b) Nunchuck seeds are assembled by hybridizing two nanotube seeds with complementary linker strands (green and purple). Nanotubes can grow from both growth sites on a nunchuck seed, producing nanotube nunchucks.

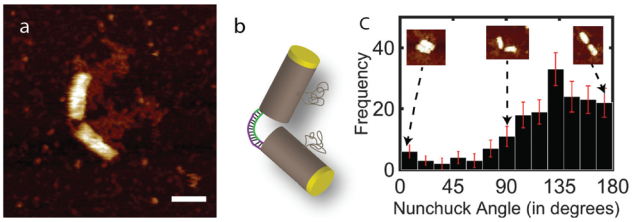

Fig. 2 (a) AFM image of a nanotube seed nunchuck. Scale bar: 50 nm. (b) Nanotube seed nunchuck model. The entangled single stranded DNA represents the unused M13mp18 scaffold not folded into the seed. It is not drawn to scale. (c) Histogram showing the distribution of angles formed by nunchuck seed structures (n = 175) after deposition on a mica surface. Error bars, generated *via* bootstrapping, represent one standard deviation.

using DNA strands designed to hybridize to specific sites on their surface. We designed a pair of partially complementary linker strands that hybridize to the origami seed at locations opposite the nanotube growth site. The design incorporates an odd number of half-helical turns in order to maximize the distance between the seed centers (Fig. 1b and S3†). Seeds with one linker strand were prepared separately from seeds with the second linker. The two nanotube seeds were then mixed to form nunchucks seeds *via* linker strand hybridization (Fig. 1b). We separated dimerized nunchuck seeds from monomeric nanotube seeds using electrophoresis through an agarose gel stained with ethidium bromide (Fig. S7,† Experimental section). Relative intensities of the dimer and monomer bands in the gel (Fig. S7†) indicated that yield of the hybridization reaction was ~25%.

We first used this strategy to construct homogeneous nanotube nunchuck seeds (see Experimental section). Atomic force micrographs (Fig. 2a and S15†) confirmed that the extracted nunchuck seeds consisted of two nanotube seeds with the expected 64 by 21 nm dimensions[22] connected by a linker of a length 27.9 ± 2.9 nm (n = 5), consistent with the expected 90 base-pair (58 base-pair linker + 16 base-pair double stranded attachment region on either side) linker length of 29.7 nm. For nanotube nunchucks to work as a tool for measuring the bend angles of the linker embedded within them, it is essential that the nunchuck be able to explore all possible angles that could from between the nanotubes. The relative orientation of the linked nanotubes in nunchuck seeds ranged from almost straight to roughly 0° (Fig. 2c). A preference for unbent configurations is consistent with the fact that the length of the double-stranded DNA linker between the nanotube seeds is less than its persistence length.

To create nanotube nunchucks, we mixed 40 pM of purified nunchuck seeds with 40 nM of REd–SEd nanotube tiles.[22] The tiles were labeled with Cy3 fluorescent dye molecules on the 5′ end of their central strand, which is well removed from the sticky ends (Note S1†). For contrast, nanotube seeds were labeled by ATTO647N-conjugated strands hybridized to an unused region of the M13mp18 scaffold that emerges from the middle of the seed wall, well removed from both the linker-presenting and the nanotube-nucleating facets (Note S6†). To prevent continued nanotube nucleation and growth during room-temperature imaging, we added guard strands that remove the short, sticky-end bearing strands (yellow and green, Fig. 1a) from free DAE-E tiles and nanotube ends.[22,24] Guard strands thus inhibit new nanotube growth without destabilizing existing nanotubes during the imaging period (Note S5†).

Fluorescence micrographs showed that two nanotubes grew from many of the nunchuck seeds (Fig. 3a, b and d). AFM images confirmed that the two nanotubes in a nunchuck were connected by nunchuck seeds (Fig. 3c and S16†). As observed in previous studies,[8,22] DAE-E tile DNA nanotubes opened on the mica surface due to electrostatic interaction between the mica surface and DNA, while origami seeds remained intact.

While most seeds in the resulting mixture grew nunchucks, we observed very few nunchucks overall. We suspected adsorption to the walls of the test tubes in which the nunchucks were prepared was responsible for the low final concentration. We found that including bovine serum albumin (BSA) in our reaction solutions increased the number of seeds observed in nunchuck preparations, presumably because non-specific adsorption of seeds to the walls of the reaction tubes was reduced (Note S7†). At the same time, the presence of BSA also increased the number of unseeded nanotubes we observed, possibly because BSA altered the energetics of nanotube nucleation and growth. Such alteration of nanotube kinetics can be expected as the presence of BSA likely also prevented tiles from adsorbing to the walls of the reaction tubes, thereby increasing the overall concentration of tiles in solution. Increasing the temperature at which tiles were incubated with nunchuck seeds from 32 °C to 34 °C effectively suppressed

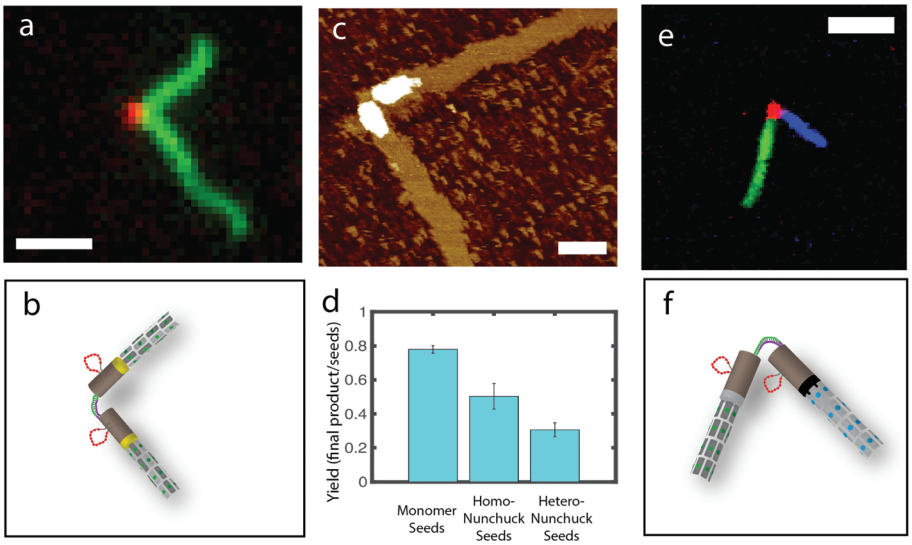

Fig. 3 Nanotubes grow from both arms of nunchuck seeds. (a) Fluorescence micrograph of a homogeneous (REdSEd) nanotube nunchuck. Nunchuck seeds are labeled with ATTO 647N (red) and REd and SEd nanotube tiles with Cy3 (green). Scale bar: 2 μm. (b) Interpretation of the nunchuck in (a). Green and blue dots on nanotubes and seeds represent the fluorescent dyes used to visualize the structures and are colored to distinguish the different dyes. Red loops show the unfolded scaffold region with hybridized fluorescent dye strands. (c) AFM image of a homogeneous nanotube nunchuck. Scale bar: 100 nm. (d) Assembly yields, defined as the fraction of nunchuck or monomer seed structures from which the designed number and type of nanotubes grew. Yields were measured using fluorescent micrographs taken at random locations on microscope slides. Error bars are one standard deviation. (e) Fluorescence micrograph of a heterogeneous (REs and SEs) nunchuck. REs tiles are labeled with ATTO 488 (blue), SEs tiles with Cy3 (green) and nunchuck seeds with ATTO 647N (red). Scale bar: 2 μm. (f) Interpretation of the nunchuck in (e).

unseeded nucleation while allowing nanotubes to grow reliably from nunchuck seeds.

Analysis of fluorescence micrographs taken at random locations showed that 50 ± 5% of nunchuck seeds formed nunchucks, 45 ± 5% had only one attached nanotube and 5 ± 2% had no attached nanotubes (n = 175). Assuming nanotubes grow from each facet on a nunchuck seed with equal probability, a 50% proportion of two-tube nunchucks implies a probability for nanotube growth on a facet of p = sqrt (0.50 ± 0.05) = 0.71 ± 0.03. This probability is consistent with the proportion of one nanotube arm observed (2 × (0.71)(0.29) = 0.41), as well as the proportion of nunchuck seeds with no nanotube arms (0.29^2 = 0.08). Single seeds nucleate nanotubes at a slightly higher rate (78 ± 2%). A small fraction of monomer seeds that remained after gel purification could account for this slight difference (Note S12†).

We next synthesized heterogeneous nunchucks (see Experimental section), *i.e.* nunchucks with two different types of nanotube arms (Fig. 3e, f and S19†). Having two different sets of DNA sequences that comprise the two arms of the nunchucks allows the arms to present either different fluorescent labels, as we demonstrate, or to have distinct functionalities. Heterogeneous nunchuck seeds consisted of a linked pair of origami seeds that were identical to those used in constructing homogeneous nunchucks, except one seed was made with adapter sequences compatible with nanotubes constructed from one type of tile, termed REs, while the other seed was made with adapter sequences compatible with a second tile type, termed SEs (see Note S1† for REs and SEs tile sequences). As before, the two seeds were prepared separately and then mixed to form nunchuck seeds *via* linker hybridization and purified by agarose gel electrophoresis.

REs and SEs tiles were designed previously[8] to have sticky ends with minimal crosstalk. Accordingly, when REs and SEs tiles were annealed together, no nanotubes consisting of both tile types were observed (Note S10†).

In experiments involving only REs tiles and seeds, 87 ± 3% seeds grew nanotubes, and in experiments involving only SEs tiles and seeds, 90 ± 2% of seeds grew nanotubes. Given these nucleation rates, the yield of heterogeneous nanotube nunchucks (30 ± 4%) was significantly less than expected. However, we also found that the yields of REs and SEs nanotubes from heterogeneous nunchuck seeds were lower than from monomer seeds. When only REs tiles were present, 67 ± 6% of heterogeneous nunchuck seeds grew nanotubes and when only SEs tiles were present, 60 ± 5% of heterogeneous nunchuck seeds grew nanotubes. These respective yields were consistent with observed yield of heterogeneous nunchucks (Note S12†).

We hypothesized that heterogeneous nunchucks grew with lower than expected yields because when the seeds for both types of nanotube are present, the adapter tiles that distinguish the nucleating facets for the two types of nanotubes may dynamically rearrange. As a result, some facets may present a mixture of binding sites for the two types of nanotubes (Fig. S12†). Neither type of nanotube would nucleate as easily from such mixed templates. This hypothesis was supported by the presence of nunchucks with two arms of the same nanotube type (4% of the observed structures).

To directly test whether dynamic "switching" of adapter strands was responsible for the low yield, we characterized the proportion of REs nanotubes that grew from monomeric seeds made with REs adapters when free SEs adapters were also present. SEs adapters lowered the yield of REs nanotubes to 70 ± 4%. A similar reduction in nanotube yield for SEs nanotubes (80 ± 2%) was observed in the presence of free REs adapters (Note S9†). Adapter switching therefore likely accounts for some, but not all, of the reduced yield of heterogeneous nunchucks over homogeneous ones. Other possible reasons for reduced yield include incomplete linker hybridization during the annealing process, which would make nunchuck seeds susceptible to dissociation and recombination. A recent study[25] suggests that longer incubation times of the individual nanotube seeds prior to co-incubation for assembly of the nunchuck seed structure could address this problem by minimizing kinetic traps that prevent hybridization from going to completion. Minor interference between the two types of tiles, REs and SEs, could also interfere with nucleation kinetics and result in lower yields. While such routes to increasing nunchuck yields merit exploration, yields of 30% are sufficient for use of individual nunchucks as mechanical magnifiers of the bending dynamics of the embedded DNA strand. For other applications, improved yields of heterogeneous nunchucks might be achieved by using distinct origami seeds for each of the different nanotubes in a desired superstructure, although such an approach would increase the complexity of the nunchuck design and the cost of purchasing the component DNA sequences.

Conclusions

This paper demonstrates a bio-mimetic strategy for hierarchically self-assembling nanotube architectures. The resulting structures have micron-scale arms that are readily visible using standard epi-fluorescence techniques. The strategy we used to assemble these structures could also be extended in order to form more complex arrangements of nanotubes, such as by increasing the number of arms in the structure. Rigid nanostructures with multiple growth sites could be used to create joints with well-defined angles. Finally, the capacity to organize nanotubes both by nucleating them and by attaching structures at their growth ends could make it possible to assemble qualitatively more elaborate architectures. To assemble such higher-order structures with high yields, it will be important to understand and correct for the causes of decreased nucleation of nanotubes from seed complexes *vs.* nucleation from single seeds.

Experimental section

DNA strands and reagents

DNA tile, staple, linker and adapter strand sequences are in the ESI.† All strands were synthesized by Integrated DNA Technologies, Inc. except M13mp18 (P-107, Bayou Biolabs). Tile, linker and adapter strands were purchased PAGE purified. Reactions were performed in TAE buffer (40 mM Tris-acetate, 1 mM EDTA, pH 8.3) with 12.5 mM magnesium acetate (TAE/Mg^{2+} buffer) unless mentioned otherwise. To prevent adsorption of DNA to PCR tubes, 0.15 mg ml^{-1} BSA biotin (A8549, Sigma-Aldrich Co.) was added during nanotube nunchuck growth (ESI Note S7†).

Nunchuck seed structure synthesis

Two solutions each containing M13mp18 (10 nM), staple strands (100 nM), adapter strands (100 nM) and one of the linker strands (10 nM) were separately annealed from 90 °C to 20 °C at −1 °C min^{-1}. To form nunchuck seeds, these solutions were combined in a single thermocycler tube at 32 °C for 12 hours (homogeneous) or 4 days (heterogeneous). The mixture was then run through a 1% agarose gel with 1.25 μg ml^{-1} ethidium bromide stain at 100 V for 1 hour and the dimer band was extracted using a Freeze N' Squeeze DNA Gel Extraction Spin Column (Biorad).

Growing nanotube nunchucks

Tile and seed labeling strands were mixed in TAE/Mg^{2+} buffer containing 0.15 mg ml^{-1} BSA-biotin to minimize adsorption of DNA to the PCR tube walls.[26] Samples were held at 90 °C for 5 min, then cooled from 90 °C to 45 °C at −1 °C min^{-1}, held at 45 °C for 60 min, then cooled from 45 °C to 34 °C at −0.1 °C min^{-1}. Gel-purified nunchuck seeds were added at 40 °C. After the anneal, the samples were held at 34 °C for 15 hours to allow for nanotube growth.

Fluorescence microscopy

2 μl of 4 μM guard strands were added to 20 μl of annealed nanotube mixture at 34 °C and incubated 1 minute just before imaging (Fig. S8†). Samples were transferred to glass slides. A cooled CCD camera (iXON3, Andor) attached to an inverted microscope (Olympus IX71) using a 60×/1.45 NA oil immersion objective captured epi-fluorescence images. Multiple images at the same location were acquired using filters for Cy3, ATTO647N and ATTO488 dyes, processed to correct for uneven illumination and superimposed to produce multicolor images. To estimate yields using fluorescence images, on average at least 2 independent experiments and a total of 10 images captured at random locations were used to measure the assembly yields described in the paper. Error bars in the measurements represent one standard deviation of the yields observed between different captured images.

Atomic force microscopy

Guard strands were mixed with samples as in fluorescence microscopy experiments. Seed labeling strands were not added to the nanotube seed nunchuck samples used for AFM imaging. 10 μl of the sample was then transferred to a freshly cleaved mica puck on which 100 μl of TAE/Mg^{2+} buffer had been added and incubated for 2 min. The mica was then washed with TAE/Mg^{2+} buffer to remove excess DNA tiles.

Image acquisition was performed on a Dimension Icon (Bruker) using Scanasyst mode and Sharp Nitride lever (SNL10-C, Bruker) probes. Images were flattened by subtracting a linear function from each scan line using Nanoscope analysis software.

Author contributions

Abdul M. Mohammed, Lourdes Velazquez, Deborah K. Fygenson and Rebecca Schulman designed the experiments and did the experimental analysis. Abdul M. Mohammed, Lourdes Velazquez and Allison Chisenhall conducted the experiments. Daniel Schiffels was involved with the conception of the system. All the authors discussed the results and wrote the manuscript.

Acknowledgements

The authors would like to thank D. Agrawal and E. Franco for valuable discussions and advice on the manuscript. This research has been supported by NSF CAREER award 125387, DOE grant DE-SC0010595 (reagents, supplies), UCSB startup funds and private donations.

Notes and references

1 G. M. Whitesides, J. K. Kriebel and B. T. Mayers, in *Nanoscale Assembly*, Springer, 2005, pp. 217–239.
2 D. Whang, S. Jin, Y. Wu and C. M. Lieber, *Nano Lett.*, 2003, **3**, 1255–1259.
3 H. T. Maune, S. P. Han, R. D. Barish, M. Bockrath, W. A. Goddard, P. W. K. Rothemund and E. Winfree, *Nat. Nanotechnol.*, 2010, **5**, 61–66.
4 M. Hazani, F. Hennrich, M. Kappes, R. Naaman, D. Peled, V. Sidorov and D. Shvarts, *Chem. Phys. Lett.*, 2004, **391**, 389–392.
5 A. M. Nguyen and C. R. Jacobs, *Bone*, 2013, **54**, 196–204.
6 E. Karsenti and I. Vernos, *Science*, 2001, **294**, 543–547.
7 S. Gadde and R. Heald, *Curr. Biol.*, 2004, **14**, R797–R805.
8 P. W. K. Rothemund, A. Ekani-Nkodo, N. Papadakis, A. Kumar, D. K. Fygenson and E. Winfree, *J. Am. Chem. Soc.*, 2004, **126**, 16344–16352.
9 F. A. Aldaye, P. K. Lo, P. Karam, C. K. McLaughlin, G. Cosa and H. F. Sleiman, *Nat. Nanotechnol.*, 2009, **4**, 349–352.
10 J. C. Mitchell, J. R. Harris, J. Malo, J. Bath and A. J. Turberfield, *J. Am. Chem. Soc.*, 2004, **126**, 16342–16343.
11 P. Yin, R. F. Hariadi, S. Sahu, H. M. T. Choi, S. H. Park, T. H. LaBean and J. H. Reif, *Science*, 2008, **321**, 824–826.
12 O. I. Wilner, R. Orbach, A. Henning, C. Teller, O. Yehezkeli, M. Mertig, D. Harries and I. Willner, *Nat. Commun.*, 2011, **2**, 540.
13 X. Y. Gao and H. Matsui, *Adv. Mater.*, 2005, **17**, 2037–2050.
14 R. Djalali, Y. Chen and H. Matsui, *J. Am. Chem. Soc.*, 2002, **124**, 13660–13661.
15 J. Couet, J. D. Samuel, A. Kopyshev, S. Santer and M. Biesalski, *Angew. Chem., Int. Ed*, 2005, **44**, 3297–3301.
16 A. V. Pinheiro, D. Han, W. M. Shih and H. Yan, *Nat. Nanotechnol.*, 2011, **6**, 763–772.
17 R. D. Mullins, J. A. Heuser and T. D. Pollard, *Proc. Natl. Acad. Sci. U. S. A.*, 1998, **95**, 6181–6186.
18 J. D. Rotty, C. Wu and J. E. Bear, *Nat. Rev. Mol. Cell Biol.*, 2013, **14**, 7–12.
19 J. Azimzadeh and W. F. Marshall, *Curr. Biol.*, 2010, **20**, R816–R825.
20 T. D. Pollard and J. A. Cooper, *Science*, 2009, **326**, 1208–1212.
21 J. M. Kollman, A. Merdes, L. Mourey and D. A. Agard, *Nat. Rev. Mol. Cell Biol.*, 2011, **12**, 709–721.
22 A. M. Mohammed and R. Schulman, *Nano Lett.*, 2013, **13**, 4006–4013.
23 D. Schiffels, *Diploma*, Ludwig-Maximilians-Universität München and University of California Santa Barbara, 2010.
24 R. Schulman, B. Yurke and E. Winfree, *Proc. Natl. Acad. Sci. U. S. A.*, 2012, **109**, 6405–6410.
25 F. Kilchherr, C. Wachauf, B. Pelz, M. Rief, M. Zacharias and H. Dietz, *Science*, 2016, **353**, aaf5508.
26 M. Goebel-Stengel, A. Stengel, Y. Tache and J. R. Reeve, *Anal. Biochem.*, 2011, **414**, 38–46.

